Silicon Electrolyte Interface Stabilization (SEISta)

Quarter 3 Report, FY20

Anthony Burrell

National Renewable Energy Laboratory
15013 Denver West Parkway
Golden, CO 80401
Phone: (303) 384-6666
E-mail: anthony.burrell@nrel.gov

Brian Cunningham, DOE-EERE-VTO Program Manager

Hybrid Electric Systems, Battery R&D
Phone: (202) 586-8055
E-mail: brian.cunningham@ee.doe.gov

Table of Contents

Overview

This report documents the Silicon Electrolyte Interface Stabilization team's approach in 1) characterizing the early-stage silicon solid-electrolyte interphase (SEI) including progress on identifying the specific reaction pathways present in the formation of the SEI layer, and 2) establishing a procedure for measuring SEI growth rate at fixed potentials and different cycling regimes.

Silicon is a viable alternative to graphitic carbon as an electrode in lithium-ion cells and can theoretically store >3,500 mAh/g. However, lifetime problems have been observed that severely limit its use in practical systems. The major issues appear to involve the stability of the electrolyte and the uncertainty associated with the formation of a stable SEI at the electrode. Recently, calendar-life studies have indicated that the SEI may not be stable even under conditions where the cell is supposedly static. Clearly, a more foundational understanding of the nature of the silicon/electrolyte interface is required if we are to solve these complex stability issues. A

new multi-lab consortium has been formed to address a critical barrier in implementing a new class of materials used in lithium-ion batteries that will allow for smaller, cheaper, and better-performing batteries for electric-drive vehicles. This consortium, named the Silicon Electrolyte Interface Stabilization (SEISta) project, was formed to focus on overcoming the barrier to using such anode materials. Five national laboratories are involved: the National Renewable Energy Laboratory (NREL), Argonne National Laboratory (ANL), Lawrence Berkeley National Laboratory (LBNL), Oak Ridge National Laboratory (ORNL), and Sandia National Laboratories (SNL).

The SEISta project was specifically developed to tackle the foundational understanding of the formation and evolution of the solid-electrolyte interphase on silicon. This project will have as its primary goal an understanding of the reactivity of the silicon and lithiated silicon interface with the electrolyte in lithium-ion systems. It consists of researchers from NREL, ANL, LBNL, ORNL, and SNL working toward clear unified goals. The Silicon Deep-Dive team, which focuses on the science and technology barriers in functional electrodes, is a critical partner in this work. Many of the researchers are shared between both teams, and we hold joint meetings to ensure effective communication between the teams.

The current goals of SEISta are:

1. Demonstrate ability to make model electrodes of Mg-Si Zintl compounds and compare SEI chemistry to silicon using XPS, STEM-EDS, and FTIR/Raman. **Q1 (100% Complete)**

2. Establish experiments and protocols for understanding the factors that affect safety in silicon anodes, with a specific focus on highly exothermic reactions that occur at silicon electrodes. **Q1 (100% Complete)**

3. Determine the effect that CO_2 has on the stability of SEI formation on model electrodes, but examining the changes in the nature of the SEI (XPS, FTIR/Raman, and quantitative electrochemical measurement) as a function of CO_2 concentration. **Q2 (100% Complete)**

4. Determine Zintl phase formation mechanism and its effect on SEI with model systems including Si nanoparticles, Si wafer, a-Si thin film using XPS, AFM/SSRM, STEM-EDS, and FTIR/Raman. **Q2 (100% Complete)**

5. Go/NoGo on production of tin-silicon alloys to be determined by the ability of the alloys to be prepared in 1-gram quantities and a demonstration that the alloys exhibit greater cyclic life than the pure metals alone. **Q2 (100% Complete, Decision = GO)**

6. Determine the chemistry and interfacial properties (e.g., nature of the chemical bonding at the surface of Si and the organic material) of LiPAA/Si interfaces as a function of charge (OCV, 0.8 V, 0.4 V, 0.15 V, 0.05 V) and drying temperature (100, 125, 150, 175, 200 °C). **Q3 (delayed to Q4)**

7. Determine how binder changes the stress/strain on silicon electrodes as a function of state of charge by varying Si nanoparticle size and surface functionally using both two- or three-dimensional model systems. **Q3 (delayed to Q4)**

8. Implement protocols that enable comparisons of safety responses in silicon anodes as a metric for improving safety in silicon cells. **Q3 (delayed to Q4)**

9. Publish a document that will enable other research and development groups to analyze stability of the SEI on a silicon-based anode, thus enabling developers or researchers to continually improve silicon cell stability (joint milestone with the Silicon Deep-Dive team). **Q4**

10. Understand how the nature and amount of formed/soluble SEI species varies with electrolyte, binder, and Si anode (with surface functionalization) using GC-MS, (*in-situ*) FTIR/Raman, and XPS. **Q4**

Approach

The SEISta team works to ensure that protocols for sample preparation, experimental design, and implementation as well as data reporting are consistent across the whole team. Each laboratory is working toward the same set of quarterly milestones using its own specific talents and capabilities in a concerted effort with the other team members. This joint focus results in multiple researchers interacting to produce and analyze data to ensure that individual experimental variations will not lead to erroneous results. Critical to the success of this effort is the use of standard samples that can be shared by all parties. In addition to weekly whole-team video presentations, we have held on-site face-to-face meetings each quarter for all team members and other interested parties to brainstorm and sort out issues with existing experiments and jointly develop new experimental plans.

Objectives

The critical issues that SEISta is attempting to address are:

What are the properties of the lithiated silicon/electrolyte interface?

What is the silicon SEI actually made of and what reactions are contributing to it?

How fast does the silicon SEI grow?

Does it stop growing?

Is it soluble?

Can it be stabilized?

For FY20, the team continues to focus on three broad tasks:

Materials Standardization—This task is critical to developing and deploying standardized samples and experimental procedures across the team. We will continue to provide full characterization to any new sample that is to be used for SEI studies to ensure reproducibility and full understanding of the material. This quarter's work focused on developing new oxide coatings and methods to control the thickness and density of oxide samples. In addition, work on the silicon nanoparticles has made progress with the enhancement of the materials collection and handling system in the plasma reactor. *Although this work dominated the early part of the project and is still critical to its success, it is now only a minor part of the work, and this is reflected in the relative balance of this quarterly report.*

Model Materials Development and Characterization—The nature of the electrode-electrolyte interaction in silicon electrodes is at the heart of the formation and stability of the SEI. The synthesis of well-defined silicon nanoparticles and the different chemical markups of lithiated silicon surfaces is being probed by preparing model compounds and thin films that may/can exist in silicon anodes. Lithium silicides, silicates, and other inorganic material (LiF, Li_2O) are being prepared, and their reactivity with electrolytes is being determined. These materials also act as standard spectroscopy samples for the researchers who are looking at the formation of the SEI on different silicon materials.

SEI Characterization—The overall objective for SEISta is to understand the nature and evolution of the SEI on silicon anodes. The materials standardization and model compounds will enable the researchers to systematically investigate the formation of the solid-electrode interphase using a wide variety of spectroscopy techniques—from different optical, microscopy, and electrochemistry—to determine how the SEI forms based on the nature of the silicon surface, and how it evolves over time. This section of work will continue to grow in scope as we move beyond the sample-characterization phase of the project and toward understanding the

nature and evolution of the SEI. *This part of the project now represents the bulk of the work and, as such, this quarterly report is largely reporting on work leading to this outcome*.

Part 1: Understanding the Evolution of the SEI

Glyme-Based Electrolytes on a-Silicon Thin-Film Anodes—Polarization Analysis

Guang Yang (ORNL), Gabriel Veith (ORNL), and Jagjit Nanda (ORNL)

Background

Recent study within SEISta confirms that even for the best-performing carbonate electrolyte with addition of a fluorinated carbonate additive—fluoroethylene carbonate (FEC)—a finite parasitic or leakage current always exists on amorphous silicon (a-Si) anodes. It points out the necessity of exploring new types of electrolytes beyond carbonates. Our previous corrosion-related reports have shown that glyme-based electrolytes could have better passivating properties on a-Si thin-film electrodes. Benefitting from the better SEI passivation, a-Si exhibits larger capacity and less capacity fade in glyme electrolytes relative to its carbonate counterparts. We have shown that the a-Si thin-film anode with a certain combination of the LiFSI, dimethoxyethane (DME) and fluorinated ether, fluoroether, 1,1,2,2-tetrafluoroethyl-2,2,3,3-tetrafluoropropyl ether (TTE) (denoted as LiFSI-3DME-3TTE) outperforms the best-performing carbonate electrolyte (GenII + 10 wt% FEC). However, the "failure mode" during extended galvanostatic cycling for both electrolytes has been largely underexplored. Herein, we study the polarization effect and internal resistance change using differential capacity for Si cycled in various electrolytes. GenII, GenII + 10 wt% FEC (GenF), and fluoroether-free electrolyte, 1.2M LiFSI+DME (denoted as LiFSI-DME) were used as the benchmark. A 50-nm a-Si thin-film anode was used as the model anode, and lithium metal was used as a counter electrode.

Results

Two types of representative long-term charge-discharge profiles of the glyme electrolytes with and without TTE are shown in Figure 1 (A-B). Notably, the lithiation capacity of the initial cycle for LiFSI-DME is 4975 mAh/g, larger than its GenII counterpart. These values are even higher than the theoretical lithiation capacity of Si (4200 mAh/g), indicative of the side-reaction occurrence during the first lithiation. This observation is further evidenced by the partial differential capacity curve shown in Figure 2(C-D), where a sharp irreversible lithiation peak shows at ~0.49 V vs. Li$^+$/Li in the 1st cycle, >0.2 V above the a-Si lithiation potential, ascribed to the electrolyte reduction to form an initial SEI layer and reduction of the surface SiO$_x$ species.[1] These side reactions result in a large initial irreversible capacity loss (ICL) of 39.7% for LiFSI-DME and 27.6% for GenII. The initial Inductively Coupled Plasma (ICP) value is important to estimate additional lithium loss to unveil a more accurate n/p ratio for practical design of Li-Si batteries. For glyme electrolytes, addition of TTE additive decreases the ICP to 36.4% for the LiFSI-3DME-3TTE electrolyte. On the contrary, addition of 10% FEC leads to ICP increasing to 32.8% versus GenII for carbonate electrolyte, agreeing with the higher parasitic current at early cycles for GenF in the GC-CA test (2019 Q2 report). After the 1st cycle, the delithiation capacity is slightly increased and stabilized until around the 10th cycle, followed by continuous fading to a certain value at the ending cycle, indicating that the SEI layer is constantly evolving as cycling is prolonged. The primary difference upon TTE co-solvent addition is the drastically improved capacity and capacity retention as cycles progress (2019 Q4 report), manifested by the stable partial capacity peaks in Figure 1(D) after the 1st cycle. Although the lithiation capacity of the LiFSI-DME is only 1787 mAh/g, it is increased to

3266 mAh/g for LiFSI-3DME-3TTE at 110th cycle, 15% larger than its best-performing carbonate counterpart (at 2841 mAh/g for GenF).
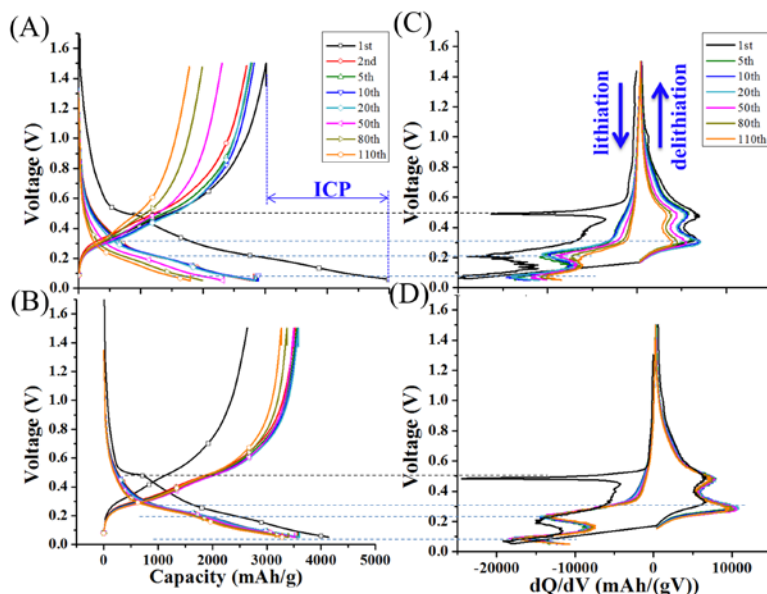

Fig. 1. Galvanostatic charge/discharge curves for a-Si anodes cycled in (A) LiFSI-DME and (B) LiFSI-3DME-3TTE. The corresponding differential capacity plots are shown in (C) and (D), respectively.
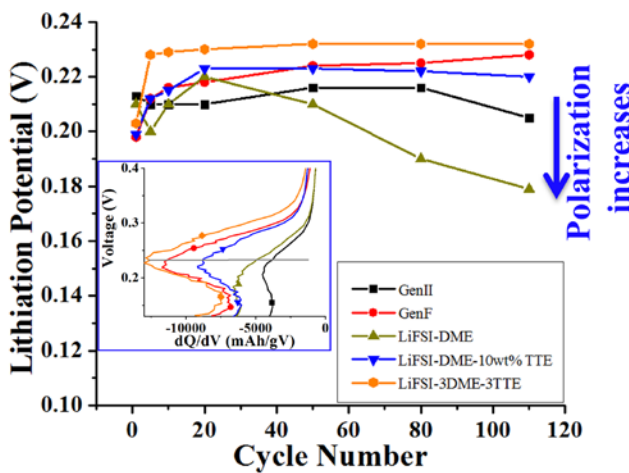

Fig 2. The lithiation potential as a function of cycle numbers for a-Si anodes cycled in various electrolytes.

LiFSI-3DME-3TTE also enables the lowest polarization effect, assuring lower energy barriers for lithiation and delithiation of a-Si. Such an observation is based on detailed exploration on the differential capacity profiles as a function of the cycle number for various electrolytes. After the 1st cycle, two lithiation peaks at ~0.07 V and ~0.20 V are observed (Figure 1(D)). For LiFSI-DME, the intensity of these two peaks continuously decreases as cycling prolongs, in accordance with the lithiation capacity fade as cycling prolongs in Figure 1(A). The similar trend is observed for two delithiation peaks at around 0.30 V and 0.49 V. Although decrease in intensity of these four peaks is > 40% for LiFSI-DME from Cycle 5 to Cycle 110, it is less than 12% for LiFSI-3DME-3TTE. Another benefit exhibited by LiFSI-3DME-3TTE that distinguishes it from the other electrolytes is its highest lithiation potential after 5 cycles shown in Figure 2, which indicates its lowest

6

polarization effect in prolonged cycles. This, in turn, allows for ease of a-Si lithiation in prolonged cycling. The passivation on the Si anode is generally considered the major driving force to increase the polarization effect upon cycling.[2] Research is ongoing on electrochemical impedance spectroscopy (EIS) of the a-Si cycled in different electrolytes for various cycle numbers to unveil the relation between the surface resistance due to SEI growth and the polarization effect for the glyme electrolytes.

Ongoing research also includes analysis of the SEI surface chemistry in a 3D manner using TOF-SIMS and depth-profile XPS, glyme SEI mechanical property analysis by nano-indentation, and local electrochemical and electronic properties of SEI formed in glyme-based by AFM-SPM (SSRM). Such studies allow us to obtain a comprehensive image of the SEI evolution on the a-Si surface in glyme electrolytes, eventually enabling general design paradigms for SEI that can effectively passivate the a-Si surface.

Conclusions

In summary, using differential capacity profiling, we further evaluate surface passivation behavior by glyme electrolytes on a-Si thin-film anodes for both early and prolonged cycling. Our results clearly show that the SEIs stemming from the glyme-based electrolytes exhibit the lowest polarization effect and the most stable cycling performance. Again, it demonstrates that glyme electrolyte with the fluorinated ether additive can passivate the Si anodes better than the carbonate counterparts.

References

1. Wu, Q., B. Shi, J. Bareño, Y. Liu, V.A. Maroni, D. Zhai, D.W. Dees, W. Lu, W., Investigations of Si Thin Films as Anode of Lithium-Ion Batteries. *ACS Applied Materials & Interfaces* **2018,** *10* (4), 3487–3494.

2. Yoon, T., N. Chapman, D.M. Seo, B.L. Lucht, Lithium Salt Effects on Silicon Electrode Performance and Solid Electrolyte Interphase (SEI) Structure, Role of Solution Structure on SEI Formation. *Journal of The Electrochemical Society* **2017,** *164* (9), A2082–A2088.

Development of *Operando* Raman Spectroscopy to Understand the Nature of Formed and Soluble Silicon-Electrolyte Interphase (SiEI) Species

Yeyoung Ha, Bertrand J. Tremolet de Villers, Zhifei Li, Andriy Zakutayev, Pauls Stradins, and Sang-Don Han

Background

Previously, we have developed an *in-situ* surface-enhanced Raman spectroscopy (SERS) technique to observe the dynamic changes of a silicon(Si)-electrolyte interphase (SiEI) and a Si anode during lithiation and delithiation.[1] With this technique, we can demonstrate how the spectroscopic changes (i.e., reversible peak intensity changes) can be correlated to the electrochemistry (i.e., state of charge, depth of discharge, and Coulombic efficiency). In addition, we can detect one of the SiEI species, alkyl carboxylate species, during cycling. To further advance the technique, we have developed a windowed coin cell for *operando* SERS measurements to overcome the challenges associated with the previous commercial *in-situ* spectro-electrochemical cell: first, the windowed coin cell requires significantly smaller amount of electrolyte to operate (~40 μL *vs* ~500 μL for the commercial cell). As the conventional $LiPF_6$-based electrolytes exhibit strong background fluorescence, reducing the electrolyte amount could decrease the background intensity and reveal the masked signals from the SiEI. Second, the windowed coin cell provides a well-controlled environment (i.e., pressure within the cell and electrolyte amount) that could permit further understanding of SiEI with respect to their natural occurrence in the battery system. Finally, as the windowed coin cells are disposable, there is negligible potential risk of cross contamination when exploring new chemistries.

Results

The windowed coin-cell design is shown in Figure 1a. A hole of 2-mm diameter was made in the center of the coin-cell cap, and a 5 × 5 mm sapphire window was epoxied inside the cap. A Cu mesh, instead of a Cu foil, was used as a current collector to enable Raman measurements through the sapphire window from the top, while allowing electrolyte to surround the electrode. Sputtered amorphous Si (a-Si) layers (30 nm) were deposited on both sides of the Cu mesh substrate (about 1-cm diameter), and it was used as a working electrode. In addition to the windowed cap and Cu mesh-based electrode, all other cell components, including the electrolyte amount (40 μL), were kept the same as a typical coin-type cell.
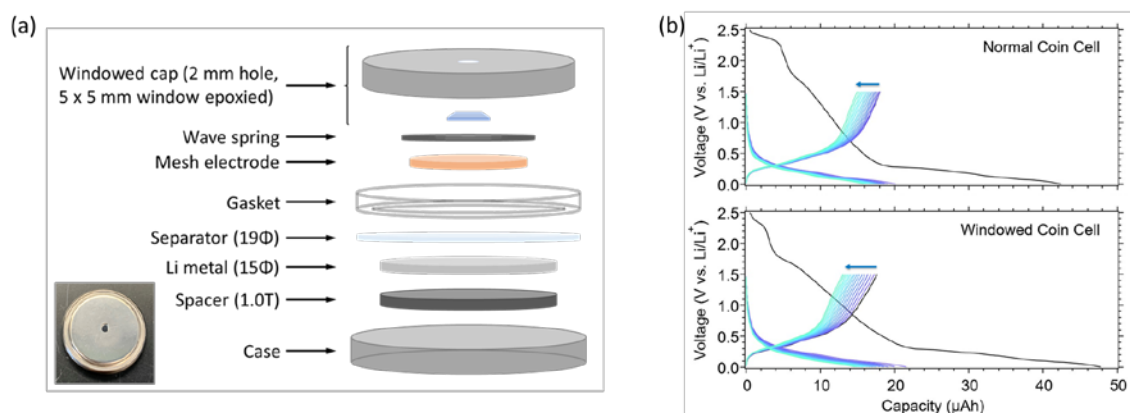

Figure 1. (a) Schematic diagram of a windowed coin cell with a photo of assembled cell as shown in the inset. (b) Voltage vs Capacity profiles of the a-Si thin-film electrodes cycled in typical (top) and windowed (bottom) coin cells. The evolution of voltage profiles during the first 15 cycles are indicated with arrows in each plot.

To evaluate the electrochemical performance of the windowed coin cell, the a-Si thin-film electrodes were cycled in both typical and windowed coin cells with a Gen2 electrolyte (1.2 M LiPF$_6$ in ethylene carbonate (EC):ethyl methyl carbonate (EMC), 3:7 wt%) in a half-cell configuration. The cells were cycled at 15-µA current in the voltage range of 0.01–1.5 V (vs Li/Li$^+$, hereafter). The evolution of voltage profiles during the first 15 cycles is plotted in Figure 1b. Compared with the electrochemical performance of a typical coin cell, the windowed coin cell exhibits a sufficient capacity retention to conduct *operando* measurements, albeit slightly faster capacity fade. All spectra presented in the report were collected using 632.8-nm He-Ne laser excitation (0.85 mW). Comparing the spectrum of an a-Si thin-film electrode collected from the windowed coin cell using a longer working-distance objective (100x/0.80NA LWD) with that obtained from the commercial cell using a 50x/0.75NA objective (Figure 2), the two spectra show similar peak positions corresponding to a-Si (at around 470 cm^{-1}), electrolyte, and Cu substrate. It is noted that the same acquisition parameters, such as 5-s exposure time and 20 accumulations, were used to collect the spectra using each cell, but the spectrum collected with the longer working-distance objective show an order-of-magnitude less intensity (the difference in y-axis scale indicated with arrows in each plot). Such behavior may be attributed to a smaller sampling volume of the 100x/0.80NA LWD objective compared to that of the 50x/0.75NA objective. In spite of lower signal-to-noise ratio, the spectral features are still visible in the spectrum collected with the 100x/0.80NA LWD objective. The spectra in this report were collected using the same acquisition parameters used in the previous experiments for comparison, but the spectral quality from the windowed coin cell can be enhanced by optimizing the parameters.
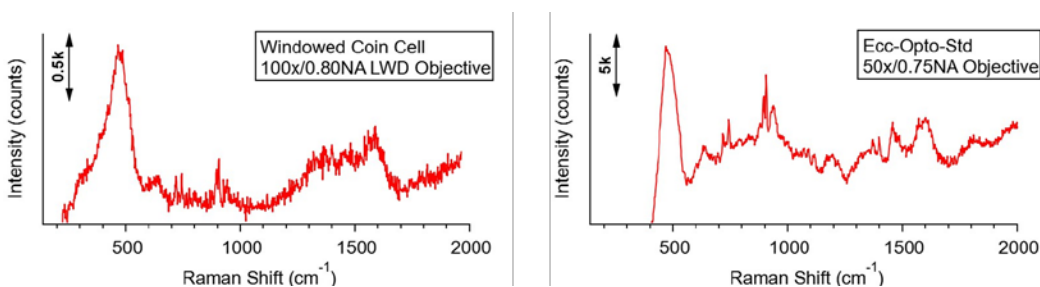

Figure 2. SERS spectra of the a-Si thin-film electrodes collected from the windowed coin cell using a 100x/0.80NA LWD objective (left) and from the commercial cell using a 50x/0.75NA objective (right). Raw spectra are shown, and the intensity counts scale (y-axis) is indicated as a vertical arrow in each plot.

Operando SERS spectra of the a-Si thin-film electrode during the first cycle were collected using the windowed coin cell (Figure 3). The a-Si peak shows a reversible behavior upon cycling: it disappears at around 0.25 V as a-Si is lithiated and re-appears at around 0.65 V as a-Si is delithiated. In addition, a peak centered at 1565 cm^{-1}, associated with alkyl carboxylate species, evolves during cycling. These features agree well with the results that we previously demonstrated using the commercial cell.[1] It is noteworthy that all raw spectra shown in Figure 3 exhibit much less fluorescence background signal associated with the electrolyte, which can be attributed to the decreased electrolyte amount and/or the smaller sampling volume of the 100x/0.80NA LWD objective.

Although we successfully reduced the fluorescence background by using the windowed coin cell with less amount of electrolyte and the longer working-distance objective with smaller sampling volume, we still could not observe the changes of additional peaks during cycling besides the a-Si and alkyl carboxylate peaks. The challenge motivates us to modify our approach by collecting the enhanced spectroscopic signals from various SiEI components. Regarding the cell configuration, we have a plan to test a thinner sapphire window (100-µm vs 330-µm current window) to minimize the signal loss from the scattering within the window. Additionally, we will prepare the samples with different methods to enhance the SERS effect: for example, the nanostructures on the Cu mesh can be tuned to maximize the plasmon resonance;[2] or the a-Si film thickness can be reduced (<30

nm) as the SERS enhancement factor exponentially decreases as a function of distance. In addition, Si electrodes can be prepared by directly depositing Si nanoparticles on the roughened Cu mesh or by casting a dilute Si nanoparticle slurry on the mesh. It is expected that these efforts can lead to a stronger SERS effect and subsequent enhanced signals from the SiEI components.
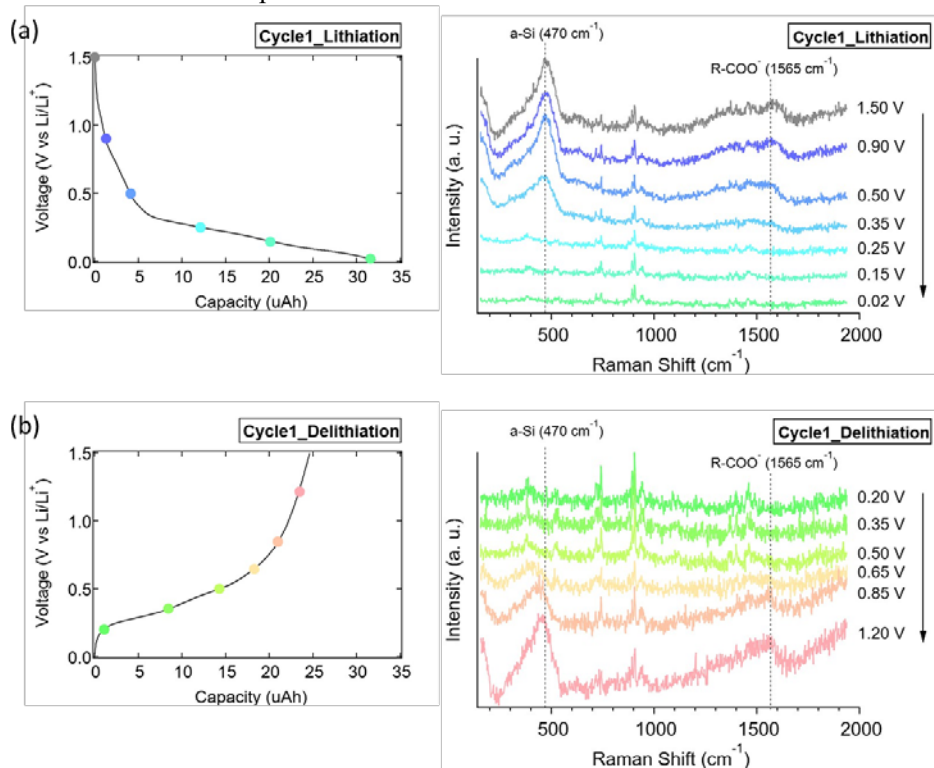

Figure 3. Voltage vs capacity profiles of a-Si thin-film electrode (left) and corresponding *operando* SERS spectra (right) collected during (a) lithiation and (b) delithiation using a windowed coin cell.

Conclusions

We have developed a windowed coin cell designed for *operando* SERS measurements and have demonstrated its reliable and reproducible electrochemical and spectroscopic performance for the a-Si thin-film electrodes. Using the windowed coin cell with less electrolyte and the longer working-distance objective with smaller sampling volume, the fluorescence background originating from the bulk electrolyte was significantly reduced. In addition, *operando* SERS spectra showed the reversible changes in a-Si peak intensity and the evolution of alkyl carboxylate species peak during cycling. We will continue our efforts to enhance signals from various SiEI components by improving the cell design, preparing the electrodes with different methods, and optimizing acquisition parameters. We believe the well-developed *operando* spectroscopic techniques will be helpful to understand how the nature and amount of formed and soluble SiEI species varies with electrolyte, binder, and Si anode (with surface functionalization) with complementary analysis using GC-MS and XPS.

References

1. Ha, Y., B.J. Tremolet de Villers, Z. Li, Y. Xu, P. Stradins, A. Zakutayev, A. Burrell, S.-D. Han, Probing the Evolution of Surface Chemistry at the Silicon-Electrolyte Interphase via In Situ Surface-Enhanced Raman Spectroscopy. *J. Phys. Chem. Lett.* **2020,** *11*, 286–291.

2. Sardari, B., M. Ozcan, Real-Time and Tunable Substrate for Surface Enhanced Raman Spectroscopy by Synthesis of Copper Oxide Nanoparticles via Electrolysis. *Sci. Rep.* **2017,** *7*, 1–11.

Understanding Mechanically Induced Interfacial Instabilities Using Controlled Deformation of Si Electrodes (LBNL)

Insun Yoon, Elisabetta Arca, Robert Kostecki (LBNL)

Background

The enormous volume change of Si during electrochemical cycling causes mechanical instabilities at various interfaces: Si-solid electrolyte interphase (SEI), Si-binder, or Si-current collector. The mechanical deformation of SEI may lead to a failure of Si surface passivation, resulting in the continuous consumption of cyclable lithium and drying of the electrolyte; disassociation between Si and binder or current collector compromises the integrity of the electrode, potentially leading to a rapid capacity fade. Thus, fundamental and quantitative understandings of Si volume-change-induced mechanical issues are highly motivated to engineer stable SEI, binder, and electrode structure.

In response, we developed an experimental platform that uses the volume change of Si as a mechanical loading mechanism to understand the mechanical instabilities. In our approach, we adopt a model of Si thin-film electrodes deposited on polydimethylsiloxane (PDMS)—a polymeric substrate. The extreme compliance of PDMS allows both lateral and vertical volume expansion of the Si thin film. From the geometry, the lateral deformation applies strain to any surface layer formed on top of the Si film. The stiff thin film on a soft substrate configuration directs the film expansion in the form of sinusoidal surface wrinkles with uniform amplitude and wavelength [1]. Thus, the applied strain can be calculated by measuring the amplitude and the wavelength, which determines the cross-sectional arc length change.

It should be noted that mechanical loading is applied by electrochemical cycling of the Si electrode; the platform could allow unambiguous electrochemical response originating from the mechanical instabilities. For the first step, we aim to understand the influence of the mechanical deformation of SEI on cycling performance.

Results

Si thin-film model electrodes are prepared by physical vapor deposition of Ti, Cu current collecting layers, and the subsequent deposition of a Si layer. The sample is assembled into a custom electrochemical cell designed for *in-situ* optical microscopy (OM). A CCD camera periodically captures the evolution of the electrode surface while a potentiostat cycles the electrode. The electrode is galvanostatically cycled 10 times at a nominal current density of 12 μA/cm^2 using the Gen2 electrolyte (LiPF$_6$ in EC:EMC =3:7 by weight).

Figure 1 presents representative OM images during the first, fifth, and tenth cycles. The initially flat topography forms two-dimensional (2D) labyrinth-like wrinkles as the Si layer biaxially expands from lithiation. At delithiated states, the wrinkled pattern vastly fades as the Si volume contracts. The remaining wrinkles may be attributed to the irreversible volume change of Si. The formation and fading of the wrinkles indicate that the softness of the substrate is allowing lateral expansion of the thin-film electrode. Such behavior appears to be repeating as the Si electrode cycles. The observation suggests that the SEI layer that formed on the Si surface is cyclically stretched and unstretched, mimicking the behavior of the practical system. Also shown in the insets are 2D fast Fourier transformation (FFT) of the corresponding OM images. The power of the 2D FFT is related to the amplitude of the wrinkles that is proportional to the surface strain. The radially averaged power of 2D FFT is extracted for each image to correlate the surface strain evolution to the state of charge.

Figure 2 presents the time evolutions of the charge and the FFT power. A clear association between the FFT power and the charge is observed: the FFT power increases at a high state of charge and decreases at a low state of charge. At a high state of charge, Si expansion induces an increase of amplitude, which is reflected by higher FFT power; the direction is reversed for the case of a low state of charge. At the current stage, the exact SEI strain cannot be measured due to the inability of optical microscopy measuring the amplitude of the wrinkles. Three-dimensional topography mapping techniques such as interferometry or scanning probe microscopy would allow an accurate measurement of SEI strain. This part remains as a future direction.
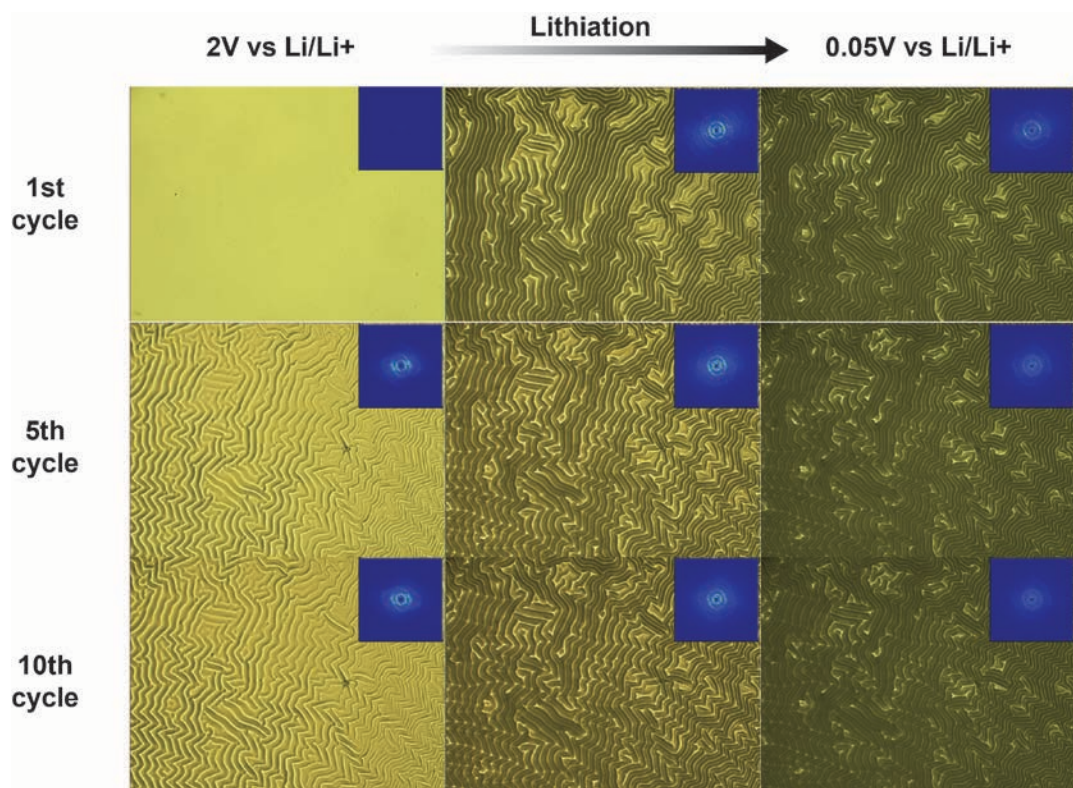

Figure 1. Optical microscope images of Si thin-film electrode at delithiated, intermediate, and lithiated states for the first, fifth, and tenth cycles. Insets are the two-dimensional fast Fourier transformation.
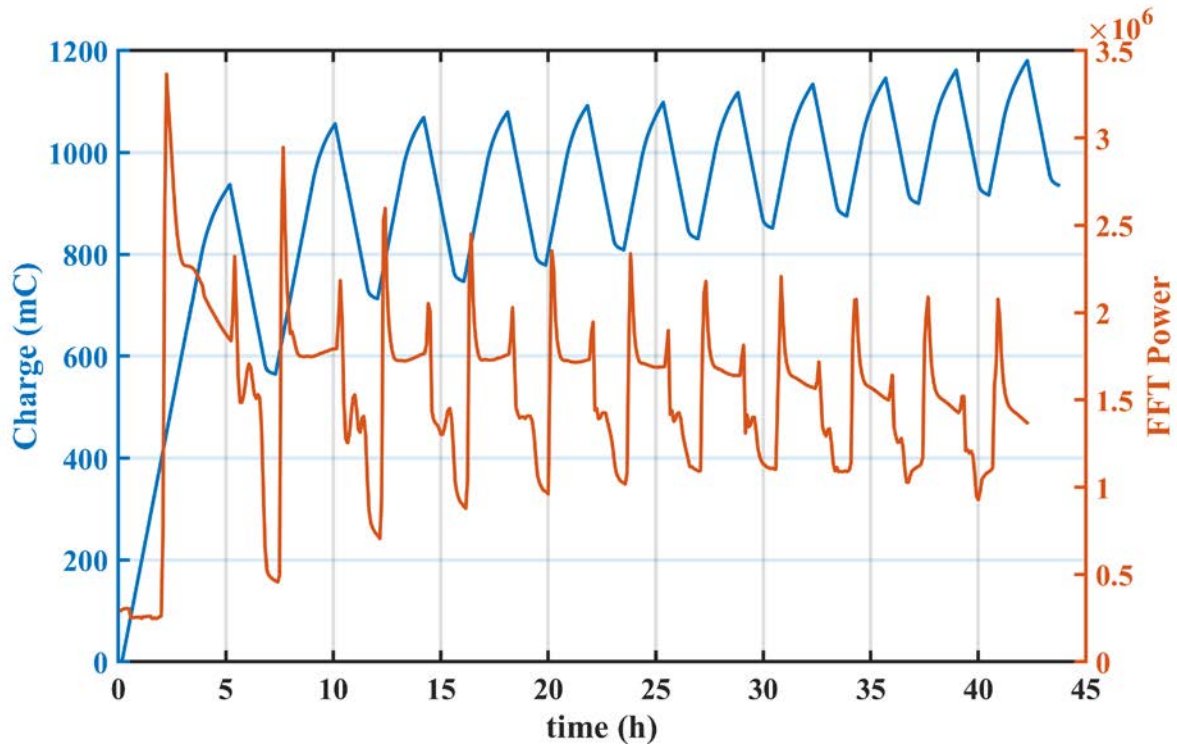
Figure 2. Time evolutions of the charge and the FFT power. The topographic and the electrochemical quantities show an evident correlation.

Conclusions

An experimental approach has been developed aimed at the fundamental understanding of mechanical instabilities associated with interfaces of Si-based electrodes. An evident lateral expansion and contraction of the Si electrode in the form of surface wrinkling is observed using optical microscopy. Such lateral deformation is reflected as the change in the amplitude. The amplitude evolution is captured by the power of 2D FFT, which shows an obvious correlation with the state of charge of the Si electrode. These series of findings serve as a demonstration that a thin-film model electrode on a polymeric substrate could potentially function as a mechanical loading mechanism by controlling the surface strain via electrochemical methods. In the forthcoming quarters, we seek to introduce structural anisotropy in the substrate to align the wrinkling pattern. Moreover, we plan to measure the three-dimensional surface topography to extract the wavelength and the amplitude of the wrinkles accurately. These future directions are expected to provide quantitative surface strain values. The immediate application of this approach will be on investigating the SEI mechanical instability. However, we expect that the platform can be extended to understand other interfacial stabilities such as Si-binder.

References

[1] Huang, Z.Y., W. Hong, Z.J. Suo, *Mech. Phys. Solids* **2005**, *53*(9), 2101–2118.

Impacts of Oxygen on the Lithiation Behavior and SEI Formation of SiO$_x$ Anodes (NREL)

Zhifei Li, Caleb Stetson, Glenn Teeter, Steve Harvey, Zoey Huey, Chun-Sheng Jiang, Mowafak Al-Jassim, and Andriy Zakutayev (NREL)

Background

Silicon materials have attracted attention due to their high theoretical capacity as anodes in lithium-ion batteries (LIBs). However, large-scale implementation has been hindered by poor cycling performance, which is partially due to large volume change during lithiation/delithiation. To alleviate the large volume change, silicon oxides (SiO$_x$) have been considered as alternatives to pure silicon electrodes. There have been some mechanistic studies about the lithiation process of SiO as anodes in LIBs; however, it is not yet fully understood how different levels of oxygen in the SiO$_x$ electrodes affect the SEI formation and its overall electrochemical performance. The presence of oxygen is almost inevitable in Si anodes where the surface of Si forms a native oxide layer when exposed to air. Different preparation processes for Si electrodes may also lead to different levels of oxygen content in the bulk Si. To investigate the effect of O content in previous quarters, we prepared model Si thin-film electrodes, including pure Si with low surface oxygen content, pure Si thin film with native oxide layer, and Si thin film with different levels of oxygen in the bulk to study the impacts of oxygen on the SEI formation and overall electrochemical performance of Si anodes. In a previous report, we demonstrated the impact of oxygen on the electrochemical behavior of the Si electrodes, where Si electrodes with higher oxygen level in the bulk exhibit a longer irreversible plateau at around 0.6 V during the first lithiation process. In this quarter report, we present additional chemical and physical characterization of pristine and cycled electrodes to further study the impacts of oxygen on the SEI formation and the lithiation/delithiation behaviors.
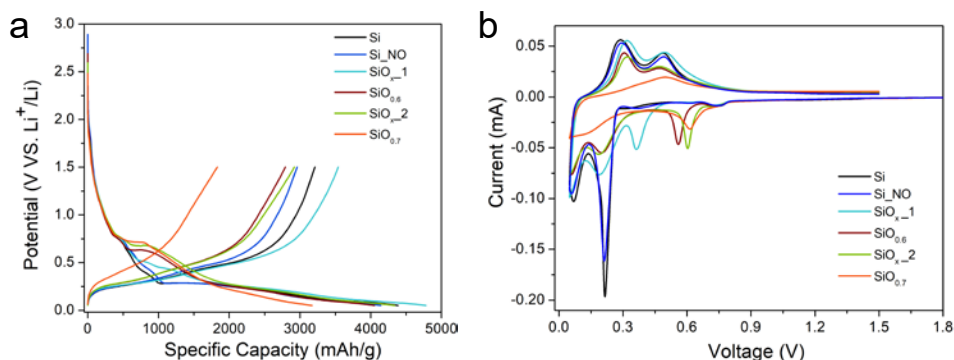
Results

Figure 1. Electrochemical characterization of Si, Si_NO, and SiO$_x$ electrodes in the potential range of 0.05–1.5 V. a) The first-cycle galvanostatic charge-discharge profiles under the current density of 1/10 C (3.9 µA/cm^2), b) The first-cycle CV curves of the electrodes tested under the scan rate of 0.1 mV/s.

The detailed preparation method of different model Si electrodes was reported in the 2019 Q3 report. In brief, six different model Si thin-film electrodes were prepared by magnetron sputtering of either a pure Si target or co-sputtering of Si and SiO$_2$ targets. For the co-sputtered Si electrodes, the oxygen level was tuned by varying the ratio between the sputtering power of the Si and SiO$_2$ targets. The thickness for all the Si and SiO$_x$ anodes reported here is around 50 nm. We selected four representative electrodes to characterize oxygen content by XPS. The pure Si electrode contains low surface oxygen (9.3 at% O, referred as Si), which quickly drops to less than 0.5 at% after several cycles of Ar$^+$ sputtering. When exposed to air, a native oxide layer will form on

14

the Si thin film (Si_NO), where the oxygen content is around 27 at%. The oxygen content of the co-sputtered Si thin-film electrodes prepared under the power combination of 90 W for Si target and 60 W for SiO_2 target is 38 at% ($SiO_{0.6}$), and the one prepared under power combination of 60 W for Si target and 90 W for SiO_2 target is 41 at% ($SiO_{0.7}$). For the SiO_x electrode prepared by the power combination of 90 W for Si target and 30 W for SiO_2 target, we referred to it as SiO_x_1, and the one prepared by 90 W for Si target and 90 W for SiO_2 target is referred as SiO_x_2. All the cells were tested in Gen2 electrolyte with 10 wt.% FEC (GenF). As shown in Figure 1a, the co-sputtered Si electrodes show an irreversible plateau in the potential range of 0.4–0.75 V, which should be due to the incorporation of oxygen in the bulk of the thin-film electrodes. The irreversible lithiation of the electrodes with higher oxygen levels in the potential range of 0.4-0.75 V is further confirmed by CV (Figure 1b). All these electrodes show two typical redox peaks of Si in the lower potential range.

To understand the cause of the irreversible plateau of the co-sputtered electrodes and the impacts of oxygen on the SEI formation of the Si anodes, we characterized the pristine electrodes and electrodes after their first lithiation to 0.55 V (vs. Li^+/Li, hereafter) and held at that potential for 1 h, with duplicate samples lithiated to a lower potential of 0.05 V. The cycled cells were disassembled in an Ar-filled glovebox and rinsed with dimethyl carbonate (DMC) with no exposure to air in the sample-transfer process. The samples were first characterized using the SSRM resistivity vs. depth-profiling technique.[1] Results summarizing the electronic resistivity of the pristine films, resistivity change from the pristine samples to the 0.55 V lithiated samples, resistivity change from the pristine samples to the 0.05 V lithiated samples, and formed SEI thickness after full lithiation are depicted in Table 1. The pristine samples show the expected result of higher electronic resistivity with higher O content. The change in resistivity from pristine to after lithiation to 0.55 V shows an interesting trend: the two thin films with the lowest O content have a minor decrease in resistivity, whereas the three thin films with nontrivial O content display a significant decrease in resistivity, proportional to the original O content. This result suggests that at 0.55 V, Si electrodes with oxygen in the bulk undergo a lithiation, whereas lithiation of Si with only surface oxygen does not proceed, resulting in a conductivity enhancement proportional to the original O content. Lithiation to 0.05 V shows a more significant conductivity enhancement for all samples, with a greater conductivity decrease for samples with higher O content. This measured conductivity increase from SiO_x to $Li_xSi_yO_z$ is consistent with experimental results established in the literature.[2, 3] SEI thickness after lithiation to 0.05 V was shown to decrease with increasing O content of the pristine electrode.

Table-1: Summary of SSRM Findings on the Pristine and Cycled Thin-Film Samples

Sample	Original Pristine Film Resistivity	Resistivity Change after Lithiation to 0.55 V	Resistivity Change after Lithiation to 0.05 V	SEI Thickness after Lithiation to 0.05 V
Si (Si/SiO_2 90/0)	~10^3 $\Omega \cdot cm$	Slight decrease	Three order-of-magnitude decrease	Thickest
Si_NO (Si/SiO_2 90/0)	~10^3 $\Omega \cdot cm$	Slight decrease	Three order-of-magnitude decrease	Thicker
SiO_x_1 (Si/SiO_2 90/30)	~10^5 $\Omega \cdot cm$	Order of magnitude decrease	Five order-of-magnitude decrease	Thicker
$SiO_{0.6}$ (Si/SiO_2 90/60)	~10^6 $\Omega \cdot cm$	Order of magnitude decrease	Five order-of-magnitude decrease	Thin
$SiO_{0.7}$ (Si/SiO_2 60/90)	~10^8 $\Omega \cdot cm$	Greater than order of magnitude decrease	Five order-of-magnitude decrease	Thin

TOF-SIMS profiles of the cycled electrodes after lithiation to 0.55 V were collected to further investigate the possible lithiation of electrodes with oxygen in the bulk. As shown in Figure 2, the Si and Si_NO electrodes only show Li-, LiO, and SiO$_2$- signal on the surface, which drop quickly along the depth of the samples; this reveals that only the surface of these two electrodes contains Li, lithium oxides, and silicon oxides, which should be attributed to SEI. In contrast, both the SiO$_{0.6}$ and SiO$_{0.7}$ electrodes exhibit Li-, LiO, and SiO$_2$- signal throughout the bulk, especially the SiO$_{0.7}$ electrode, which shows steady Li-, LiO, and SiO$_2$- signal along the depth of the sample. This result confirms the lithiation of these two electrodes at 0.55 V, whereas the Si and Si_NO electrodes only contain lithium at the surface, agreeing with the SSRM results. In addition, the presence of LiO signal in the bulk of the SiO$_{0.6}$ and SiO$_{0.7}$ electrodes indicates that the lithiation of silicon oxides would produce lithium oxides, which has been reported in the literature.[3, 4]
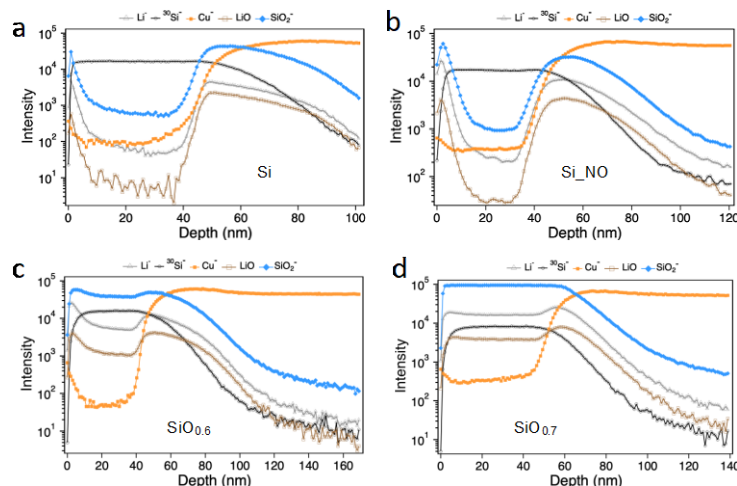

Figure 2. TOF-SIMS profiles of the Si, Si_NO, SiO$_{0.6}$ and SiO$_{0.7}$ electrodes after being lithiated to 0.55 V.

We further examined the surface properties of the cycled electrodes via XPS. The surface composition of the electrodes after the first lithiation to 0.55 V and 0.05 V is summarized in Table 2. In general, the electrodes lithiated to 0.55 V show lower carbon and oxygen content but higher F, P, and Si content. The much higher Si content suggests a thinner SEI on the electrodes at this potential than those lithiated to 0.05 V because XPS is a surface-sensitive technique, with a sampling depth of 5–10 nm. The only source of phosphorous (P) is LiPF$_6$, so the relative high P content of the electrodes at 0.55 V than at 0.05 V indicates that there are more decomposition products from LiPF$_6$ on the surface of the electrodes. After lithiating the electrodes to 0.05 V, the thickness of the SEI increases with a decrease in P and F content and an increase of the C and O content. Because the C and O composition is expected to originate from the decomposition of the electrolyte solvent molecules, the change in thickness and composition of the SEI suggests that there is more LiPF$_6$ decomposition in the higher potential range and more electrolyte solvent decomposition in the lower potential range.

Table-2: Surface Composition of Cycled Electrodes Obtained from XPS

Atomic composition (%)	C	O	F	P	Si
Si, 0.55 V	19.9	18.3	41.2	2.2	18.4
Si_NO, 0.55 V	36.8	17.0	23.2	2.8	20.2
SiO$_{0.6}$, 0.55 V	37.2	20.1	24.7	1.8	16.2
SiO$_{0.7}$, 0.55 V	25.9	17.0	41.7	1.7	13.7

Si, 0.05 V	56.0	25.4	15.4	0.79	2.47
Si_NO, 0.05 V	41.6	20.1	31.7	1.2	5.5
SiO$_{0.6}$, 0.05 V	36.9	21.8	35.0	1.2	5.1
SiO$_{0.7}$, 0.05 V	64.3	19.6	12.7	1.2	2.2

Furthermore, in the electrodes lithiated to 0.55 V, the P content decreases as the oxygen content of the electrode increases, indicating that oxygen may help suppress the decomposition of LiPF$_6$. When being lithiated to 0.05 V, the electrodes with lower oxygen content show lower Si content but higher C content except for the SiO$_{0.7}$ electrode. The lower Si content again suggests a thicker SEI of the lithiated electrodes, and the higher C content should be due to more electrolyte solvents decomposition. The deviation of the trend for the SiO$_{0.7}$ electrode indicates that it may have quite different lithiation behaviors from other electrodes. Overall, the surface composition of these electrodes lithiated to different potentials reveals the impact of oxygen content on electrolyte decomposition and formation of SEI.

Conclusions

We synthesized a series of SiO$_x$ electrodes with different oxygen levels to investigate the impact of oxygen content on the electrochemical performance of Si-based electrodes. The electrochemical characterization clearly shows the impacts of the oxygen on the lithiation and delithiation behaviors of the SiO$_x$ electrodes. SSRM characterization of the prepared thin films, in their pristine form, lithiated to 0.55 V and lithiated to 0.05 V states demonstrate a strong dependence on the original O content in the prepared electrodes. The presence of O in the original pristine electrode is correlated to a conductivity enhancement after lithiation to 0.55 V, suggesting a voltage-dependent lithiation mechanism for SiO$_x$ content. The TOF-SIMS profiles further confirm that at the lithiation potential of 0.55 V, only the electrodes that contain O in the bulk are lithiated through the bulk whereas the Si electrodes that only contain surface O do not show evidence of bulk lithiation. The SSRM results also suggest that lithiation to 0.05 V results in an increase in conductivity for all samples, representing the transformation of Si to Li$_x$Si$_y$. SEI appears to form with increased thickness on thin films with lower O content, indicating that SiO$_x$ presents less reactive surfaces for electrolyte degradation. This phenomenon is further confirmed by XPS. In addition, the XPS results also suggest that at the beginning of the lithiation, the SEI contains more inorganic products that derived from the LiPF$_6$ and that as the lithiation proceeds to lower potential, more electrolyte solvent decomposition products are contained within in the SEI.

References

1. Stetson, C., T. Yoon, J. Coyle, W. Nemeth, M. Young, A. Norman, S. Pylypenko, C. Ban, C.-S. Jiang, M. Al-Jassim, A. Burrell, Three-Dimensional Electronic Resistivity Mapping of Solid Electrolyte Interphase on Si Anode Materials. *Nano Energy* **2019**, *55*, 477–485.

2. Charles, R.J., Some Structural and Electrical Properties of Lithium Silicate Glasses. *Journal of the American Ceramic Society* **1963**, *46*, 235–243.

3. He, L.-N., J. Xua, Properties of Amorphous SiO$_2$ Films Prepared by Reactive RF Magnetron Sputtering Method. *Vacuum* **2003**, *68*, 197–202.

3. Kim, J.H., C.M. Park, H. Kim, Y.J. Kim, H.J. Sohn, Electrochemical Behavior of SiO Anode for Li Secondary Batteries. *Journal of Electroanalytical Chemistry* **2011**, *661*, 245–249.

4. Miyachi, M., H. Yamamoto, H. Kawai, T. Ohta, M. Shirakata, Analysis of SiO Anodes for Lithium-Ion Batteries. *Journal of The Electrochemical Society*, **2005**, *152*, A2089–A2091.

Part 2: Understanding Zintl Phase Stabilization of the SEI

Investigating *in-situ* Ternary Li-Mg-Si Zintl Phase Formation and Evolution

Baris Key, Xiang Li, Fulya Dogan, Niya Sa, Steve Trask , James A. Gilbert, Jack Vaughey (ANL)

Background

A stable Li-M-Si ternary phase with less chemical reactivity helps to stabilize the Si anode structure and reduce the side reactions with electrolyte, and it eventually benefits the electrochemistry. This ternary phase can be formed by adding multivalent cations (such as Mg2+, Al3+, Ca2+) in the electrolyte in an *in-situ* manner. To understand the mechanism of Zintl phases formation and its dynamics, electrochemical testing, EQCM and high-resolution ^{7}Li & ^{29}Si NMR are used on coin cells and pouch cells.

Upon discharge, two driving mechanisms are proposed:
  (a) Exchange $Li_{3.75}Si + 0.1Mg^{2+} => Li_{3.55}Mg_{0.1}Si + 0.2Li^+$
  (b) Competition $Li_{3.55}Si + 0.1Mg^{2+} => Li_{3.55}Mg_{0.1}Si$

Upon charge:
  (c) $Li_{3.55}Mg_{0.1}Si => Li_{3.55}-xMg_{0.1}Si + xLi$

Results

Previously, we have reported that Li-M-Si (M=Mg,Al,Ca, Zn) ternary phases (Zintl phases) can be formed by co-insertion of M cations in an *in-situ* fashion during lithiation process, leading to less reactive ternary lithium silicide and enhanced long-term cycling performance.[1] However, the formation mechanism and the fundamental chemistry (such as the dynamic changes upon charge and discharge behind this) is still unknown. Traditional diffraction techniques are especially sensitive to heavy atoms and those materials with long-range order, which cannot provide enough insights into the Li-related structure and the very amorphous Si phases after cycling. Nuclear magnetic resonance (NMR) is a powerful tool to determine the local structural environments of nuclei such as Li, P, or F.[2] In this work, we comprehensively study the electrochemical lithiation of Paraclete Energy Si anode at multiple charge states to gain insights into Zintl phase formation mechanisms. In addition, the electrochemical data obtained from coin cells and pouch cells agree with each other and with our former findings.

The 1st cycle electrochemical profiles, high-resolution ^{7}Li NMR spectra, and the corresponding spectral simulation from unwashed pouch cells are shown in Figure 1. Four main Li resonances are observed and analyzed: the black peak around 0 ppm is from the residual Li salts in electrolyte as well as electrolyte decompositions; the relatively sharp and narrow component at -1 ppm is assigned to Li in the surface Si-O layer; Li in isolated Si is at 8 ppm; and Li in Si clusters resonates over 13 ppm. These peak assignments are consistent with our previous *ex-situ* ^{7}Li NMR studies on coin cells. The electrochemical profiles are very similar for both Gen2+10%wt. FEC (GF) and Gen2+10%wt. FEC + 0.1M Mg(TFSI)2 (GFM) electrolyte formulations when the cells are only discharged to 100 mV, whereas GF shows slightly higher (~30 mAh/g) specific capacity. As a result, most Li ions are inserted into isolated Si (and/or extended silicon clusters) with 97.1% in GFM and 97.8% in GF. When fully discharged to 10 mV, as seen in Figure 3(a), although GF and GFM share the similar discharging profile, the GF cell holds more Li ions (~140 mAh/g) than GF. At this stage, Li insertion into Si clusters as well as possible migration form isolated Si, and eventually forms over-lithiated Si phases. Upon charge, Li extraction preferentially occurs in over-lithiated Si phases, then Si clusters, and finally, in isolated Si, which correlates well with the coin-cell data. When charged to 400 mV, GF and GFM series represent Li removal hysteresis to different extents. There is still 24.7% Li in Si clusters and

57.7% Li in isolated Si in the GFM cell, compared with almost all Li in isolated Si in the GF cell. At the fully charged state, spectra shift toward lower frequency, indicating reversible Li dynamics.
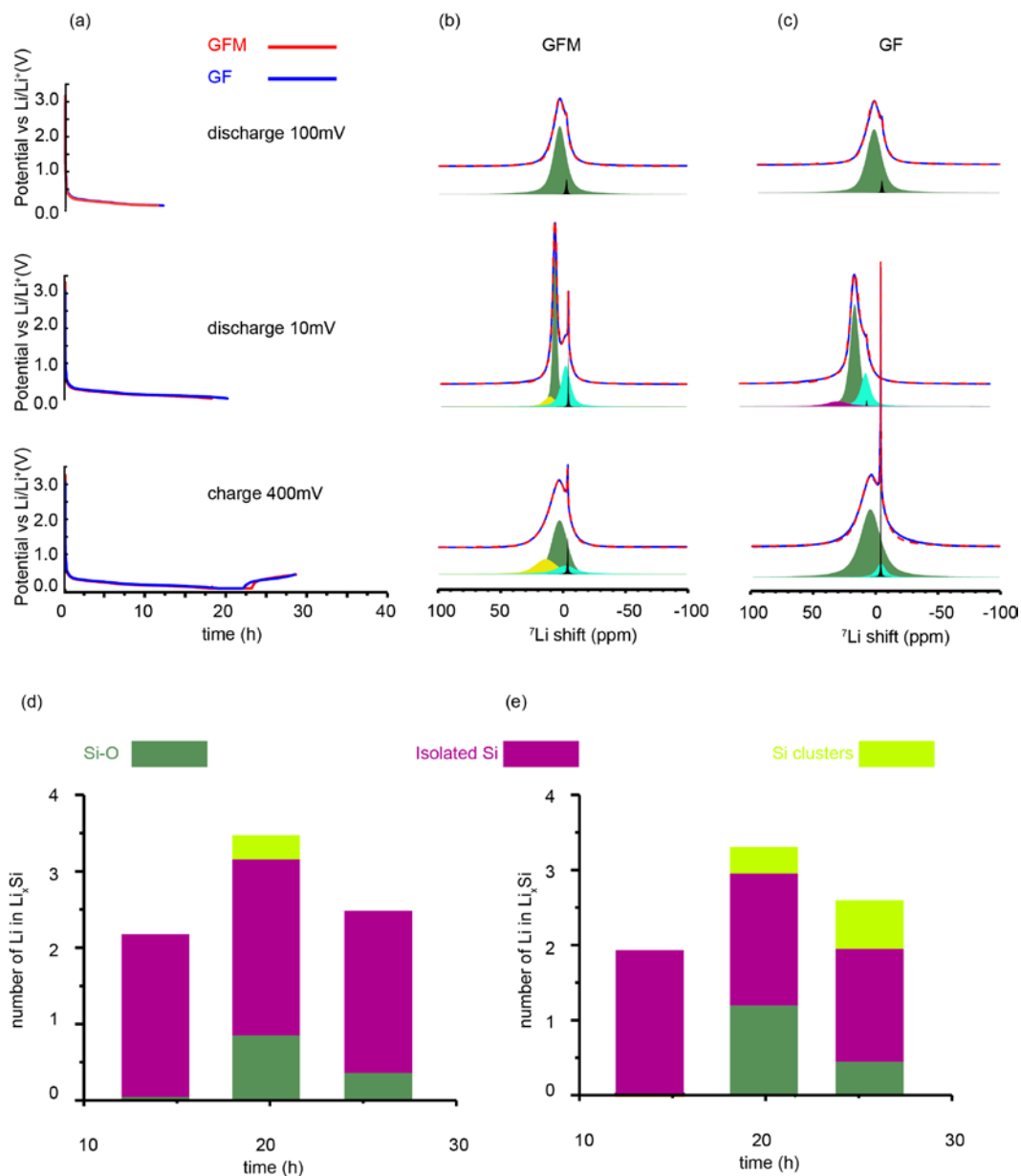

Figure 1. Electrochemical performance of GF and GFM at 100 mV, 10 mV, and 400 mV (a). Experimental data (solid line) and simulation (dash line) of GFM (b) and GF (c), Li quantification with GF (d) and GFM (e) electrolytes.

^{7}Li NMR spectra comparison between pouch cells and half cells are shown in Figure 2. At the early state (above 100 mV), there is no significant difference except broader line shape for pouch cells, which is due to the relatively lower Magic Angle Spin (MAS) rate (20 kHz) of the NMR experiment when compared with that of coin cells (60 kHz). However, at the fully discharged state, both GF and GFM spectra show significant differences compared to the results for the coin cells. More Li content was found to be in SEI and the Si-O layer in pouch cells, which is likely because pouch cells have significantly more electrolyte and greater surface

area, leading to more side reactions on the surface and SEI formation. As shown in Figure 1(b), Figure 2(b), and Figure 3, 52.9% Li in isolated Si and 10.8% Li in Si clusters indicate that theternary phase formation may require more Li insertion into Si clusters as well as over-lithiated Si. In contrast, with additional 140 mAh/g discharge capacity, the GF pouch-cell spectrum shifts to lower field and shows over-lithiated Si at 22 ppm. Longer voltage hold at 10 mV may be accelerating co-insertion of Mg^{2+} and Li-Mg-Si ternary formation in GFM cells.
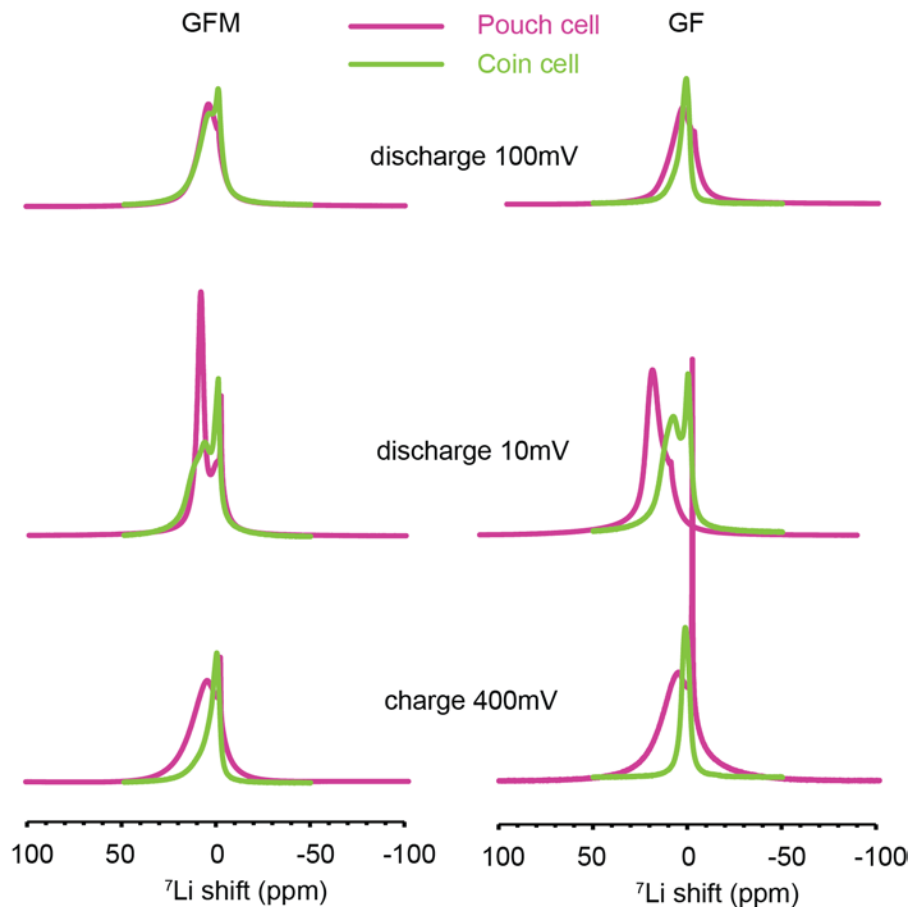
Figure 2. (a) ^{7}Li NMR spectra comparison between pouch cells (purple) and coin cells (yellow) for GFM and GF.

In Figure 3, the discharge electrochemistry of Paraclete Si is characterized by two distinct voltage plateaus at 230 mv and 100 mV, which correspond to a two-phase reaction: an irreversible dissociation of amorphous Si and a crystalline phase formation of $Li_{15}Si_4$. Voltage hold at 10 mV before delithiation is designed to break up all crystalline $Li_{15}Si_4$ and form amorphous Li_xSi upon charge, representing a broad voltage peak at 280 mV. Note that although GF and GFM share similar voltage profiles, the subtle shift toward lower voltage at 100 mV might be a sign of Mg co-insertion. During a deeper discharging process below 100 mV, Mg^{2+} could participate in lithiation to form the Li-Mg-Si ternary by two possible mechanisms:

(1) $Li_{3.75}Si + 0.1Mg^{2+} => Li_{3.55}Mg_{0.1}Si + 0.2Li^+$; Li ions continue coordinating with Si and form crystalline $Li_{3.75}Si$ first; ion exchange between Li^+ and Mg^{2+} is driven by low potential.

(2) $Li_{3.55}Si + 0.1Mg^{+2} => Li_{3.5}Mg_{0.1}Si$, which is more likely from an electrochemical perspective due to slightly lower overall lithiation capacities observed during the discharge for GFM.
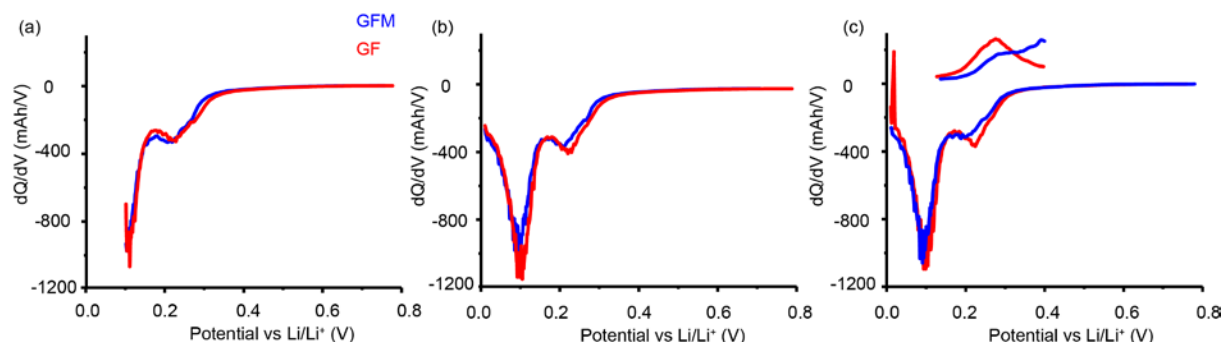
20

Figure 3. Differential capacity vs voltage plots of GF and GFM at 100 mV (a), 10 mV (b) upon discharge, and 400 mV (c) upon charge.

To further understand the mechanism of the Zintl phase formation, an *in-situ* Electrochemical Quartz Crystal Microbalance Measurement with Dissipation mode is applied to a Si thin-film anode free of binder and conductive carbon vs Li metal in two electrolyte environments, GenF and GenFM. Figure 4 presents simultaneous electrochemical lithiation voltage from open-circuit voltage (OCV) = 2.5 V to 0.015 V with the corresponding frequency difference at the 3rd overtone. Two lithiation stages are monitored: the pre-lithiation process for SEI formation from 2.5 V to 350 mV, and the post-lithiation stage from 350 mV to 15 mV. Results suggest that before lithiation occurred (>350 mV), the frequency shift for the GenFM electrolyte is less significant than for the GenF electrolyte, suggesting that the SEI formation is less prominent with the Mg addition in comparison with the GenF electrolyte. Frequency shift is mainly contributed from the electrolyte reduction as well as lithium insertion into surface SiO, in agreement with the ssNMR finding. For the post-lithiation stage (100 mV to 15 mV), the frequency shift for the GenFM electrolyte at the lowered voltage range from 100 mV to 50 mV is more significant than the GenF electrolyte; this trend is opposite, in contrast to the pre-lithiation stage. Lithiation of Si into $Li_{3.75}Si$ gives a mass increase of 48% of the reaction; however, formation of the ternary Zintl phase and the magnesiation of $Li_{3.75}Si$ to form $Li_{3.55}Mg_{0.1}Si$ phase merely gives a mass increase of 1.9%. Consequently, the apparently decreased frequency shift with the Mg addition occurring at lowered voltage range from 100 mV to 50 mV clearly suggests a partial inclusion of Mg and formation of the Li-Mg-Si ternary occurring in parallel in addition to the lithiation of Si.
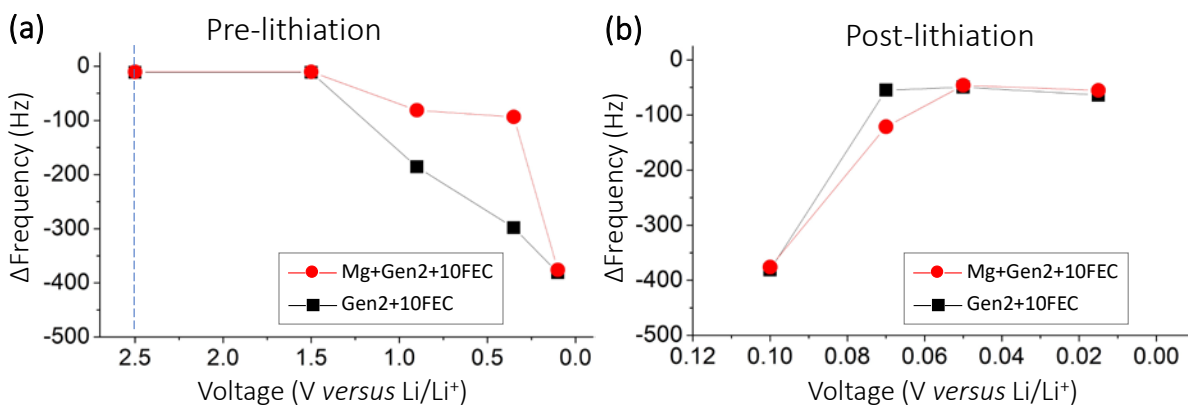

Figure 4. Correlation of the lithiation voltage versus the frequency difference from *in-situ* EQCM measurement of a 50-nm Si thin film vs lithium metal in GenF (black square) and GenFM (red circle) electrolyte. (a) Pre-lithiation stage at V>350 mV; (b) Post-lithiation stage at V < 350 mV.

Finally, limited preliminary calendar-life hold tests were performed on 80% Si CAMP electrodes in full coin cells (vs. NMC532) with the procedure in Figure 5. Comparison of parasitic currents for GF and GFM

suggests significantly better passivation for the system with magnesium, consistent with EQCM results. Immediate follow-up studies will focus on more stable cycling electrodes and long calendar-life tests using various multivalents with long cycle-life targets.
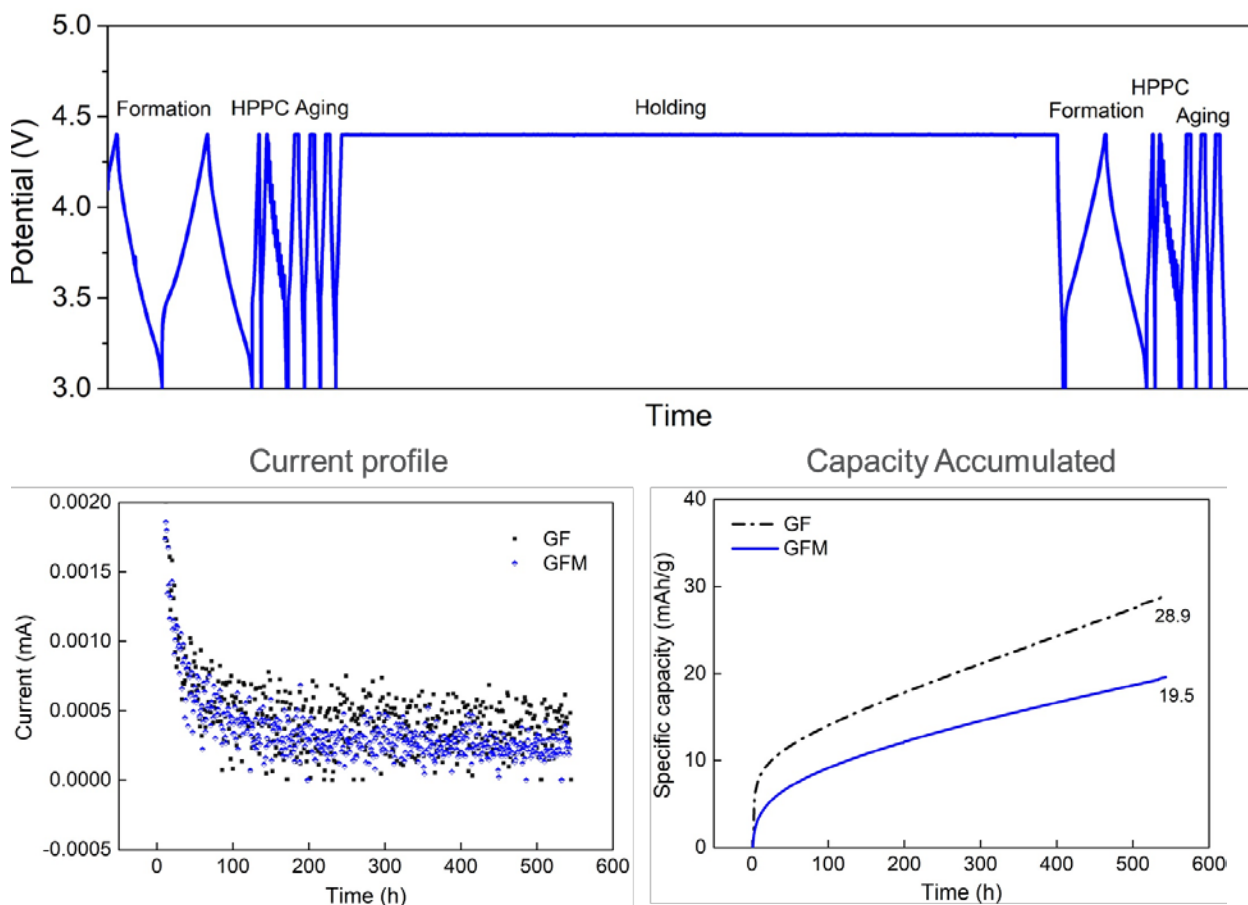

Figure 5. Preliminary calendar-life test protocol and current and capacity plots during the 540-h voltage hold step for GFM and GF electrolytes.

Conclusions

The evolution of Li and Si local environments for pure Si anode in two different electrolytes were investigated using EQCM, *ex-situ* ^{7}Li, and ^{29}Si MAS NMR. Li-Mg-Si ternary phase formation acquires a large amount of Li insertion into Si clusters. It could be accumulated by holding the voltage at sufficiently low voltage, such as 10 mV. More even Li distribution and lower electrochemical hysteresis were promoted by Li-Mg-Si ternary phase. Electrochemistry performance from scale-up pouch cells is consistent with lab-scale coin cells. We propose that upon discharge, Li-Mg-Si ternaries form uniformly, preferably by competition between Li and Mg only at deeply lithiated stages; upon charge, Mg remains in the bulk, forming Li-poor or completely lithium-deficient $Li_xMg_{0.1}Si$ phases and contributing to stable ternary phases in subsequent cycles. The promising potential for scale-up applications examined by pouch cell testing offers more stable passivation at high states of charge in full cells, which should yield longer calendar life for optimized electrodes; this will be the immediate focus in the next quarter.

References

1. Key, B. *et al.* Real-Time NMR Investigations of Structural Changes in Silicon Electrodes for Lithium-Ion Batteries. *J. Am. Chem. Soc.* **2009**, *131*, 9239–9249.

2. Pecher, O., J. Carretero-González, K.J. Griffith, C.P. Grey, Materials' Methods: NMR in Battery Research. *Chem. Mater.* **2017**, *29*, 213–242.

Part 3: Development of Standardized Tests for Calendar and Cyclic Life

Cycle and Calendar-Lifetime Protocols for Si-Based Anodes

Max Schulze, Mike Carroll, Fernando Urias, Greg Pach, Ryan Pekarek, Jaclyn Coyle, and Nathan Neale

Background

Our major FY20 metric is the Q4 Milestone: Have published a document that will enable other research and development groups to analyze stability of the SEI on a silicon-based anode, thus enabling developers or researchers to continually improve silicon cell stability (joint milestone with the Silicon Deep Dive). This document will be used by the community to evaluate where new materials, electrolytes, and electrode architectures positively affect the cycle and calendar lifetimes on an apples-to-apples basis. Specifically, these protocols should:

- Be accomplished in short timeframes (~1 week)
- Measure critical metrics necessary to determine if lifetime requirements can be met (no cheating)
- NOT necessarily provide fundamental knowledge, i.e., they are a "sniff-test" to determine if the material is worth investigating/developing further
- Distinguish between:
    - Active material loss
    - Lithium inventory loss (main limiting factor)
    - Electrolyte degradation.

Results

In Q2, we began initial studies based on the knowledge gained over the many years of work on protocol development for other electrodes and the Si Deep Dive and SEISta projects. Preliminary experiments were designed and executed, then refined based on the results through a multi-lab effort. Then, the SARS-CoV-2 pandemic struck, and all work was shut down. Thankfully, NREL was able to prioritize work on this critical Milestone at its earliest stages of re-opening in Q3. Below, we summarize the results from those extensive sets of experiments conducted in Q3 and progress toward this critical Q4 Milestone.

Cycle Lifetime. Half-cells with unlimited Li-ion inventory exhibit capacity loss only from 1) active material loss by any mechanism or 2) electrolyte degradation. Many literature reports show long cycle
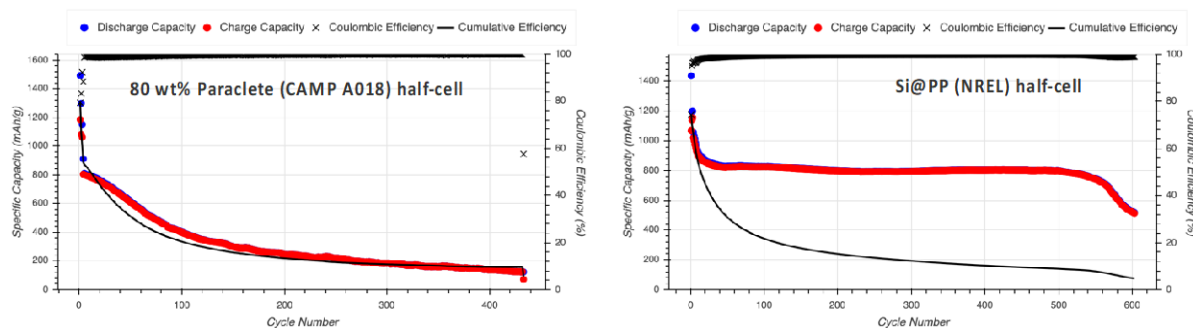

Figure 1. Left: 80 wt% Paraclete (CAMP A018) ~150-nm-diameter NP half-cells exhibit a decline in reversible capacity that derives almost exclusively from active material loss. Right: Si@PP (PECVD Si NPs functionalized with phenylphenol) ~30-nm-diameter NP half-cells show some early-cycle active material loss in the first tens of cycles, but transitions to stable reversible capacity for hundreds of cycles; Rollover capacity decline at cycle ~500 eventually occurs owing to electrolyte consumption. For both types of active material, the cumulative efficiency, not the Coulombic efficiency, shows that neither system is stable.

lifetimes in half-cells, indicating good retention of active material. However, half-cell data where Coulombic efficiency is scaled 0%–100% conveys minimally useful information about Li-ion consumption by electrode, which is a degradation mode not well captured by half-cells. Cumulative efficiency, which is the Coulombic efficiency summed over n cycles, is a much more relevant parameter, allowing material stability to be evaluated. As shown in Figure 1, the solid black trace is the cumulative efficiency and can be used to distinguish active material loss from electrolyte degradation mechanisms. In half-cells with an unlimited Li-ion inventory, capacity decline that tracks the cumulative efficiency indicates active material loss, whereas high >99.5% Coulombic efficiency only shows that the active material has stabilized, not the SEI. Additional electrolyte/Li-ion consumption is accurately described by plotting the cumulative efficiency.

We have applied this methodology to a number of different electrode active materials. Shown in Figure 2 are both Coulombic and cumulative efficiency plots for half-cells of various Si, graphite, and LFP electrodes. Note that the anodes are polarized to 10 mV vs. Li/Li$^+$ except 80 wt% pSi (electrodes from CAMP), which was cycled to 100 mV vs. Li/Li$^+$. In all Si-based electrodes, high >99.5% Coulombic efficiency after cycle 130 is somewhat irrelevant because the decline in cumulative efficiency to <20% at this cycle number is the critical parameter, showing that none of these Si-based electrode/electrolyte systems are viable.
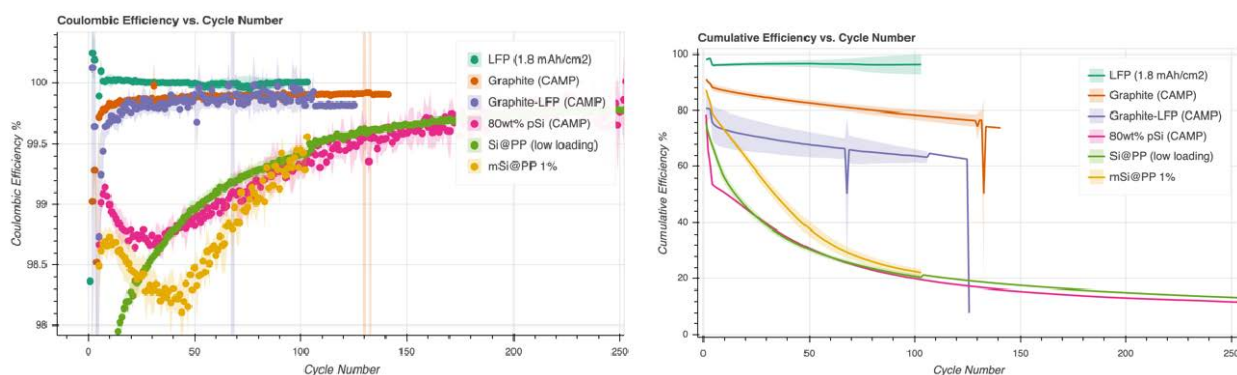

Figure 2. Half-cell data for a variety of electrodes (graphite-LFP is full-cell). All anodes were cycled to 10 mV vs. Li/Li$^+$ except 80 wt% pSi (CAMP), which was cycled to 100 mV vs. Li/Li$^+$ (3.35 V vs. LFP). Left: Coulombic efficiency. Right: Cumulative efficiency.

Full cells present a very different picture. We explored full cells with both an excess and a limited Li-ion inventory. Lithium iron phosphate (LFP) was chosen as the cathode because it maintains a very flat voltage profile over a wide state of charge (SOC), minimizing the need to account for voltage variations or use a reference electrode. Li-ion inventory was controlled by varying the n/p ratio < 1 (excess Li) or > 1 (limited Li). Figure 3 shows the effects of these two different n/p ratios. More stable reversible capacity is observed with excess Li-ion inventory (n/p < 1). In this case, although Li is still being consumed, the excess amount of total Li relative to the Si-based anode and the relatively flat voltage profile of LFP—along with a fixed cutoff potential—allows that Si to achieve nearly the same SOC and only a gradually declining reversible capacity over the duration of the experiment. In contrast, full cells with limited Li-ion inventory (n/p > 1) exhibit an immediate and steady capacity decline that tracks the cumulative efficiency. Together, these experiments reveal the significant Li-ion inventory consumption that occurs with cycling.

Calendar Lifetime. How do we measure Li-inventory consumption during calendar aging while minimizing perturbation of the electrode by cycling (i.e., mechanically stressing the Si and SEI)? To answer this critical question, we evaluated several different electrochemical cycling strategies. A test published in the USABC protocols[1] measures capacity in Li-ion limited full-cells before and after long (~1-month) OCV time. However, this test is too long to allow a rapid feedback loop required for evaluating new active materials, electrolytes, and electrode designs. To avoid this lengthy feedback loop, we developed and evaluated several methodologies and have narrowed in on a protocol that measures current (and thus capacity loss) during a voltage hold rather

than at OCV. The integrated current can be extrapolated to long timeframes, which provides a predicted calendar lifetime out to years from this short <2-week test.
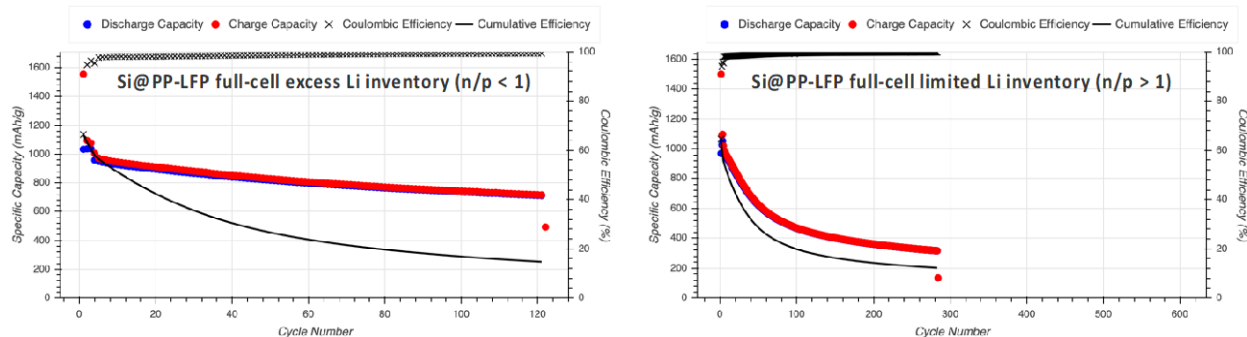

Figure 3. Left: Si@PP (PECVD Si NPs functionalized with phenylphenol) full-cells with a n/p ratio < 1. Right: Si@PP full-cells with a n/p ratio > 1.

The full details of this protocol will be communicated in the Q4 Milestone report, but initial experiments appear to validate this approach, as shown in Figure 4. A full-cell using LFP with n/p < 1 is constructed, and after three formation cycles (ensuring that the active material is lithiated and delithiated), the anode is charged to between 10 and 100 mV vs. Li/Li$^+$ (3.44 to 3.35 V vs. LFP). The electrode is then charged to the top of SOC, and the voltage is held for 180 h. The current is monitored during this extended voltage hold, as shown in the middle panel of Figure 4. The right panel in Figure 4 is the analysis of the current during the voltage hold, which is an exponential fit to these data and provides the time in years at which the delithiation capacity is 80% of its initial value.
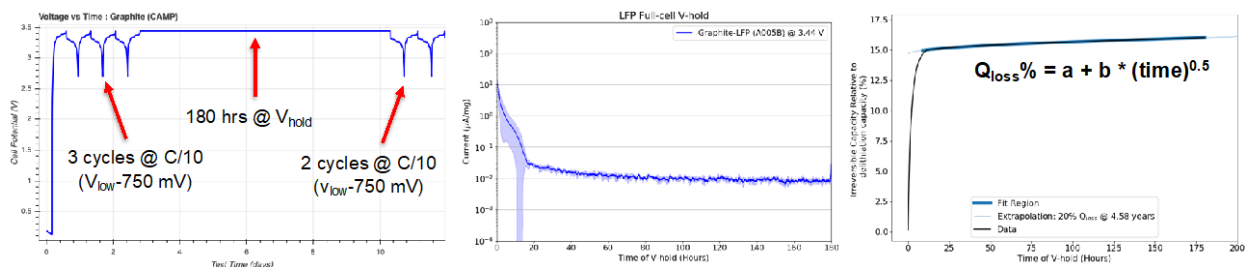

Figure 4. Voltage-hold protocol for rapid determination of cell calendar lifetime. Left: Potential–time plot of protocol. Middle: Current–time plot during V_{hold}. Right: Delithiation capacity loss during V_{hold} calculated from current–time data and equation used to fit the linear portion of the curve and extrapolate the calendar lifetime.

We have tested this protocol for graphite and a variety of different Si-based electrodes, SOCs, and excess vs. limited Li-ion inventory full cells. As shown in Figure 5, the graphite-based electrodes exhibit the highest calendar lifetime exceeding 5 years, with all Si-based electrodes giving far worse calendar lifetimes of <3 years. These data are consistent with the expected result (graphite is more stable than Si) and provide confidence that this approach is valid; however, these results are very preliminary and need full validation. We are running a bevy of additional tests to determine uncertainty in 1) measuring diminishingly small currents, 2) extrapolating <180 h of data to multi-year lifetimes, and 3) ensuring that this methodology actually is measuring Li-ion consumption rates that affect calendar lifetime. For instance, we are collecting long-term (many-cycle) cycling and voltage-hold experiments as one set of validation experiments.
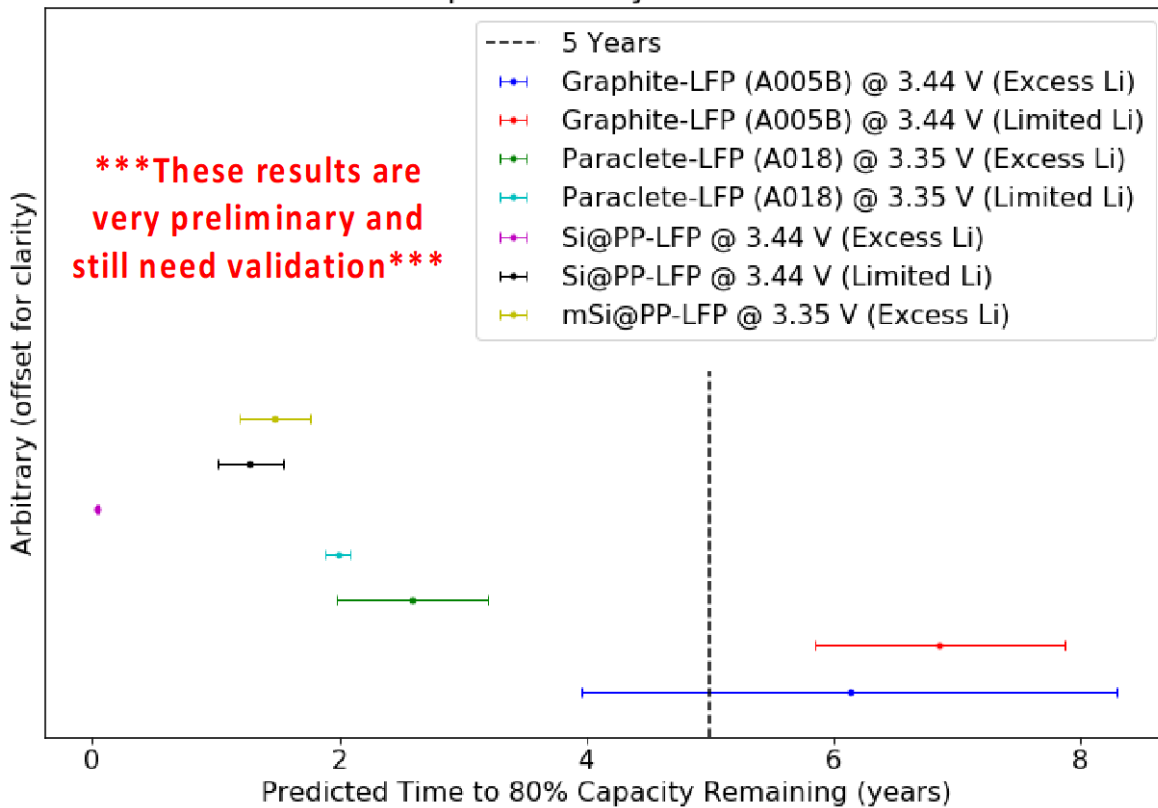
Figure 5. Preliminary data using the calendar-lifetime protocol shown in Figure 4 for a variety of electrodes, SOCs, and excess vs. limited Li-ion inventory.

Conclusions

In Q3 of FY20, we have made major progress toward our critical Q4 Milestone. A cycle-lifetime protocol was developed in which full-cell Si anode/LFP cathodes are used to monitor the cumulative efficiency. Active-material degradation vs. electrolyte degradation can be established using this protocol and provides a simple and straightforward method of comparing advances in electrode/electrolyte systems on cycle lifetime. A rapid calendar-lifetime protocol was developed that initial data suggest provides a multi-year prediction of this more challenging parameter. Validation experiments of this calendar-lifetime protocol are underway to establish the accuracy and preciseness of this approach.

References

[1] https://www.uscar.org/commands/files_download.php?files_id=405